Classical solutions for a free particle in a confocal elliptic billiard

Miguel A. Bandres and Julio C. Gutiérrez-Vega[a)]
Photonics and Mathematical Optics Group, Tecnológico de Monterrey, 64849, México

(Received 1 August 2003; accepted 24 October 2003)

The classical dynamics of a free particle constrained to move in an integrable two-dimensional confocal elliptic billiard is investigated. We derive the characteristic equations for periodic orbits, classify the orbits, present the Poincaré maps, give expressions for the lengths of the trajectories, and do a stability analysis of special orbits. We also explore some interesting geometrical constructions for the billiard which can be extended to the confocal elliptic billiard. The latter provides a well-motivated and relatively straightforward example of Hamilton–Jacobi theory, elliptic integrals, and Jacobi elliptic functions in a way that is seldom discussed in the undergraduate curriculum.
[DOI: 10.1119/1.1634967]

I. INTRODUCTION

The billiard problem is stated as follows. A particle in the interior of a region bounded by perfectly reflecting walls is given an initial velocity, and the problem is to calculate and understand the resulting trajectory. Despite the simplicity of the statement of the problem, its solution is not simple in many cases. Indeed, in recent years the study of classical and quantum billiards has witnessed a revival of research interest. The evidence of strong connections between the periodic orbits in a classical system and the spectrum of quantized energy levels of the corresponding quantum system has helped us understand the chaotic and nonchaotic properties of classical and quantum systems in the semiclassical limit.[1] Two-dimensional (2D) billiards have became popular because progress in nanotechnology has led to the fabrication of very small closed structures (quantum corrals), which can be used to confine electrons.[2] The boundary of the nanodevices is sharp enough that the electron can be regarded as a free particle confined within a 2D billiard with infinite walls.

The dynamical behavior of the billiards is highly dependent on the geometry of the boundary. Rectangular and circular shapes are examples of integrable systems,[3–5] while the Bunimovich stadium and Sinai billiards are completely chaotic.[6] Intermediate situations, that is, systems with both integrable and chaotic behavior, are the most common type of billiards.[7] Billiards involving rectangular and circular geometries are well-treated in education-oriented journals[3–8] and some textbooks,[9,10] but the elliptic geometry has not been discussed in this context.

The dynamics of a free particle moving in a 2D planar billiard bounded by a smooth convex closed boundary has been widely studied.[8,11–16] Formal proofs have been obtained to support the conclusion that the elliptic boundary is the only integrable smooth planar billiard for any value of the eccentricity.[17]

The integrability of a billiard is usually evidence of the existence of underlying symmetries. For example, a Hamiltonian system with n degrees of freedom is integrable if it has n constants of motion. For the elliptic billiard, one constant of motion is the total energy E, and another is the scalar product of the angular momenta with respect to the foci $\Gamma = \mathbf{L}_1 \cdot \mathbf{L}_2$.[18] Conservation of energy says almost nothing about the dynamics of the periodic orbits of the particle. In contrast, the constant Γ is the key to understanding the dynamical behavior of the particle and classifying its orbits.

In addition, there has been some studies of the dynamical properties of convex smooth billiards with inner concave scatterers.[19] In most cases the presence of the scatterer leads to strong chaos in the system. However, for the elliptic billiard with the inner scatterer a confocal ellipse, Γ remains constant under the convex reflections at the internal ellipse. It follows that this billiard geometry is an integrable system whose dynamical behavior is regular and predictable.

The aim of this paper is to study the classical periodic orbits for a free particle in a confocal elliptic billiard. The principal result is a derivation of the characteristic equations for describing the periodic trajectories and calculating the orbit lengths. We solve these characteristic equations for several situations and explore some interesting geometrical constructions for the confocal elliptic billiard.

The motivations for analyzing this system include the fact that the classical periodic orbits for the confocal elliptic billiard have a richer phase-space structure than the corresponding purely elliptical case,[11–16] the pattern of allowed periodic trajectories varies dramatically as the eccentricities of both ellipses are varied, and the confocal elliptic billiard may be considered as a generalization of the annular billiard discussed previously by Robinett.[5] We studied the confocal elliptic billiard originally in order to analyze the statistical properties of its quantum mechanical energy spectrum, in particular, the distribution of the level spacings. A global qualitative and quantitative knowledge of the classical dynamics is important for understanding the correspondence to the quantum mechanical spectrum. However, the classical dynamics of this system is an interesting example of the phenomena of integrable systems in its own right.

The study of the classical confocal elliptic billiard may be valuable to undergraduate students for several reasons. Contrary to the rectangular, circular, and annular billiards where the conditions for periodic orbits can be derived using only geometrical arguments, the solution in the elliptic case requires the use of Hamilton-Jacobi theory, which is a standard technique for analyzing conservative systems whose motion is periodic. Despite its applicability, Hamilton-Jacobi theory often is not discussed in undergraduate courses of mechanics or is applied only to well-known central force problems such as the pendulum, the 2D harmonic oscillator, and the Kepler problem.[20,21] The confocal elliptic billiard is a nontrivial example of the application of the Hamilton–Jacobi theory involving non-central forces.

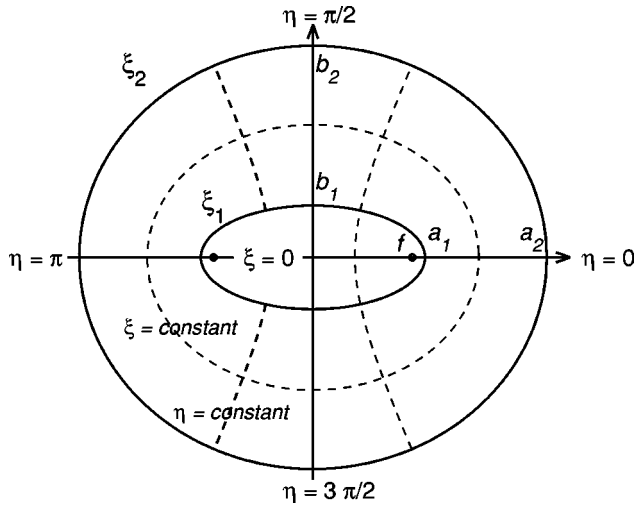

Fig. 1. Geometry of the confocal elliptic billiard. Lines of constant ξ are ellipses and lines of constant η are hyperbolae.

The characteristic equations for the confocal elliptic billiard can be expressed in terms of elliptic integrals or Jacobi elliptic functions. Even though elliptic integrals arise in many problems of undergraduate physics (for example, the simple pendulum and the off-axis electric potential of a uniform charged ring), students are usually unfamiliar with them.

Due to the special form of the characteristic equations for periodic orbits, it is possible to translate their analytical properties into interesting geometrical constructions for the confocal elliptic billiard. Because computing elliptic integrals and Jacobi elliptic functions can be done using commercial mathematical software, most of the results presented in this paper can be reproduced by students with a minimum of programming experience. The paper is relatively self-contained and students can take our results as a starting point to explore numerically the properties of elliptic integrals and how they predict interesting geometrical properties of the orbits inside the billiard.

II. CLASSICAL DYNAMICS OF THE CONFOCAL ELLIPTIC BILLIARD

The geometry of the confocal elliptic billiard is shown in Fig. 1. We shall study the dynamics of a point particle moving freely in the interior and obeying the reflection law at the boundaries. The elliptic boundaries are given by

$$\frac{x^2}{a_j^2}+\frac{y^2}{b_j^2}=1, \quad j=1,2, \tag{1}$$

where a_j and b_j are the semimajor and semiminor axes of the jth ellipse and $a_1<a_2$ (see Fig. 1).

The system has two degrees of freedom and two constants of the motion,[11] the total energy E, and the scalar product of the angular momenta about the foci of both ellipses, $\Gamma=\mathbf{L}_1\cdot\mathbf{L}_2$. In general, the motion of the particle can be characterized in terms of the canonical coordinates q_i and canonical momenta p_i. The trajectory of the particle is restricted to move in phase space (q_i,p_i) such that E and Γ remain constant. An effective method of handling the periodic trajectories is provided by the application of action-angle variables in Hamilton–Jacobi theory. In Hamilton–Jacobi theory terminology, the constants of motion are called the action variables of the system and are often represented as $J_i(q_i,p_i)$. For each $J_i(q_i,p_i)$, there exists a corresponding angle variable designated by $\Theta_i(q_i,p_i)$. The action variable J_i is given by

$$J_i=\frac{1}{2\pi}\oint p_i\,dq_i, \tag{2}$$

where the integral $\oint$ is over a complete period of the coordinate q_i. The angle variable Θ_i corresponds to the frequency ω_i of the periodic motion of the coordinate q_i and is given by

$$\omega_i\equiv\frac{d\Theta_i}{dt}=\frac{\partial H(J,\Theta)}{\partial J_i}, \tag{3}$$

where H is the Hamiltonian of the system. In the 2D billiard, the periodic trajectories are determined by the requirement that ω_1/ω_2 must be equal to a rational number n/r, where n and r are integers. A detailed treatment of Hamilton–Jacobi theory can be found in Refs. 20 and 21.

We formulate the confocal elliptic billiard problem in elliptic coordinates

$$x=f\cosh\xi\cos\eta, \quad y=f\sinh\xi\sin\eta, \tag{4}$$

so that the focal points are at $x=\pm f=\pm(a_j^2-b_j^2)^{1/2}$. Lines of constant ξ are ellipses and lines of constant η are hyperbolae. The boundaries of the confocal elliptic billiard are the ellipses $\xi=\xi_j=\operatorname{arctanh}(b_j/a_j)$ with eccentricities

$$\epsilon_j=\frac{f}{a_j}=\operatorname{sech}\xi_j. \tag{5}$$

We also introduce the convenient parameter

$$\mu_j\equiv\frac{b_j}{f}=\sinh\xi_j. \tag{6}$$

The velocity of the particle in terms of elliptic coordinates is

$$\mathbf{v}=h\frac{d\xi}{dt}\hat{\xi}+h\frac{d\eta}{dt}\hat{\eta}, \tag{7}$$

where $h(\xi,\eta)=f(\cosh^2\xi-\cos^2\eta)^{1/2}$ is the metric factor of the coordinates ξ and η, and $\hat{\xi}$ and $\hat{\eta}$ are the elliptic unit vectors related to the Cartesian unit vectors by

$$\begin{pmatrix}\hat{\mathbf{x}}\\ \hat{\mathbf{y}}\end{pmatrix}=\frac{f}{h}\begin{pmatrix}\sinh\xi\cos\eta & -\cosh\xi\sin\eta\\ \cosh\xi\sin\eta & \sinh\xi\cos\eta\end{pmatrix}\begin{pmatrix}\hat{\xi}\\ \hat{\eta}\end{pmatrix}. \tag{8}$$

For the conservative billiard, the Lagrangian L for a particle of mass M equals its kinetic energy, that is, $L=\frac{1}{2}Mh^2[(d\xi/dt)^2+(d\eta/dt)^2]$, and the Hamiltonian H is equal to the total mechanical energy E of the particle. Both can be written in terms of elliptic coordinates as

$$L=\frac{1}{2}Mh^2\left[\left(\frac{d\xi}{dt}\right)^2+\left(\frac{d\eta}{dt}\right)^2\right], \tag{9}$$

$$H=E=\frac{P^2}{2M}=\frac{1}{2M}\left(\frac{p_\xi^2+p_\eta^2}{h^2}\right), \tag{10}$$

where $P=(2ME)^{1/2}$ is the constant magnitude of the linear momentum of the particle, and the canonical momenta are

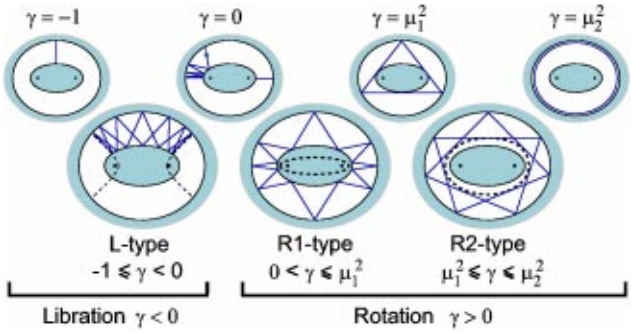

Fig. 2. Classification of the orbits in the confocal elliptic billiard. The dashed lines represent the caustics of the tori.

$$p_\xi = \frac{\partial L}{\partial \dot{\xi}} = Mh^2 \frac{d\xi}{dt}, \tag{11a}$$

$$p_\eta = \frac{\partial L}{\partial \dot{\eta}} = Mh^2 \frac{d\eta}{dt}. \tag{11b}$$

The second constant of the motion is the product of angular momenta about the foci:

$$\Gamma = \mathbf{L}_1 \cdot \mathbf{L}_2 = (\mathbf{r}_1 \times M\mathbf{v}) \cdot (\mathbf{r}_2 \times M\mathbf{v}), \tag{12}$$

where $\mathbf{r}_1 = (x-f)\hat{\mathbf{x}} + y\hat{\mathbf{y}}$ and $\mathbf{r}_2 = (x+f)\hat{\mathbf{x}} + y\hat{\mathbf{y}}$. By using Eqs. (7) and (8), we can easily obtain Γ as a function of the elliptical coordinates and momenta

$$\Gamma = M^2 f^2 h^2 \left[\left(\frac{d\eta}{dt} \right)^2 \sinh^2 \xi - \left(\frac{d\xi}{dt} \right)^2 \sin^2 \eta \right]$$

$$= \frac{f^2}{h^2} (p_\eta^2 \sinh^2 \xi - p_\xi^2 \sin^2 \eta). \tag{13}$$

The conserved quantity Γ is a useful parameter for characterizing the motion of the particle. For the confocal elliptic billiard the range of Γ is limited to $-(Pf)^2 \leqslant \Gamma \leqslant (Pb_2)^2$, where the lower limit, $\Gamma_{\min} = -(Pf)^2$, corresponds to the vertical motion along the y-axis and the upper limit, $\Gamma_{\max} = (Pb_2)^2$, corresponds to the sliding orbit (limiting motion along the outer boundary). It is convenient to normalize Γ by defining an dimensionless constant of motion, γ, given by

$$\gamma \equiv \frac{\Gamma}{P^2 f^2}, \tag{14}$$

in the interval $[-1, \mu_2^2]$. We will see that γ assumes a special role in the description of the orbits in the confocal elliptic billiard.

If we use Eqs. (10) and (13), the canonical momenta (11) can be rewritten in terms of the conserved quantities (P, γ) as

$$p_\xi = Pf\sqrt{\sinh^2 \xi - \gamma}, \tag{15a}$$

$$p_\eta = Pf\sqrt{\sin^2 \eta + \gamma}. \tag{15b}$$

For the confocal elliptic billiard we identify three kinds of orbits, depending on the value of γ (see Fig. 2).

(1) *Libration* (L): $-1 \leqslant \gamma < 0$. This motion involves an oscillation in the coordinate η, such that the particle is confined to an area delimited by the two elliptic boundaries and two branches of confocal hyperbolic caustics with curves $\eta = \eta_C$ and $\eta = \pi - \eta_C$, as shown in Fig. 2. The extension of each chord of the trajectory intersects the x axis between the foci. The special value $\gamma = -1$ represents the isolated stable orbit along the y axis.

(2) *Rotation* (R): $\gamma > 0$. The particle goes around the inner ellipse such that the coordinate η increases (or decreases) without limit. The confocal elliptic billiard has two kinds of rotational motion as shown in Fig. 2.

(a) R1: $0 < \gamma \leqslant \mu_1^2$. The particle bounces alternately off each ellipse and hence ξ is in the interval $[\xi_1, \xi_2]$. The extension of each chord of the trajectory touches an elliptic caustic inside the inner boundary. The special value $\gamma = \mu_1^2$ represents the tangential trajectory to the inner boundary, which is not necessarily a periodic orbit.

(b) R2: $\mu_1^2 \leqslant \gamma \leqslant \mu_2^2$. The particle rotates, bouncing only at the outer ellipse. The tori avoid the interior of the elliptic caustic $\xi = \xi_C > \xi_1$, touching its boundary between every two consecutive reflections at the outer boundary. This case is the same as the rotational motion in a classic elliptic billiard.

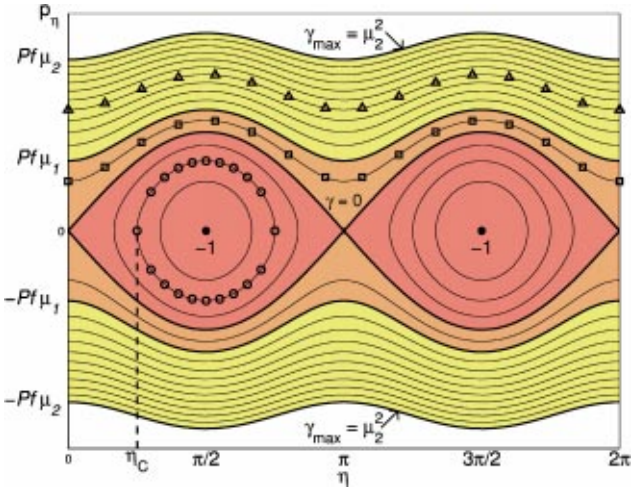

Fig. 3. Poincaré mapping (η, p_η) for the confocal elliptic billiard. The form of the lines is given by $\gamma = \text{constant} = (p_\eta / Pf)^2 - \sin^2 \eta$. Specific orbits are represented by circle markers for L motion, square markers for R1 motion, and triangle markers for R2 motion.

A complete knowledge of a dynamical system can be reached only by exploring its phase space. Usually, the practical way of doing this is to introduce a surface of section and to investigate the Poincaré mapping defined by the flow. For the billiard the natural coordinates of the map are the angular coordinate η and the tangential momentum p_η. They are canonically conjugate, which means that the Poincaré map is area preserving. Additionally we will explore the map constructed with the radial coordinate ξ and the radial momentum p_ξ.

Figures 3 and 4 show the phase diagrams (η, p_η) and (ξ, p_ξ) for the confocal elliptic billiard. The lines are level curves corresponding to constant values of γ in Eq. (15). These expressions are two-valued functions corresponding to the two possible signs of the momenta. The particle is restricted to move in a specific trajectory in phase space where E and γ remain fixed. Each phase diagram exhibits three regions related to a specific kind of motion of the particle.

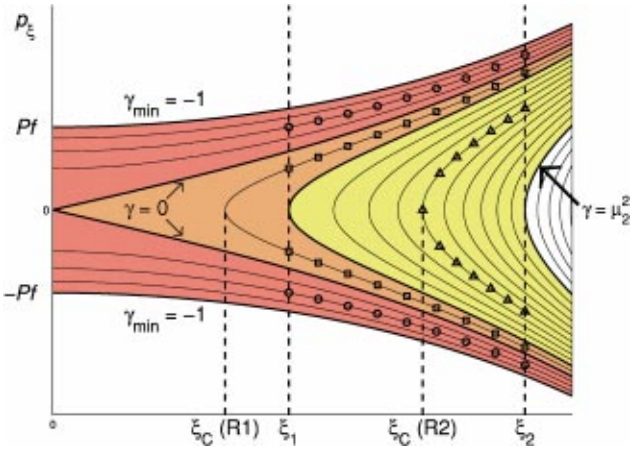

Fig. 4. Poincaré mapping (ξ, p_ξ) of the confocal elliptic billiard. The form of the lines is given by $\gamma = \text{constant} = \sinh^2 \xi - (p_\xi/Pf)^2$.

The separatrix between the libration and the rotation motions is defined by the curves $\gamma = 0$. An orbit on the separatrix is characterized by straight segments whose extensions pass through one or the other focus between consecutive reflections (see Fig. 2). The unstable isolated periodic orbits at the two saddle points $(\eta, p_\eta) = (0,0)$ and $(\pi,0)$ perform an oscillation along the x axis. In the plane (η, p_η), the lines inside the separatrix correspond to the librational motion with $\gamma < 0$, and the lines outside the separatrix correspond to the rotational motion with $\gamma > 0$. The separatrix for motions R1 and R2 is at the level curve $\gamma = \mu_1^2$.

We can follow the motion of the particle along some of the iso-γ curves in phase space. For instance, a libration motion corresponds to closed orbits (circle markers) in the plane (η, p_η) exploring a restricted range of η while repeatedly touching two hyperbolic caustics. The turning-point (nearest the p_η axis) defines the caustic $\eta = \eta_C$. On the other hand, in the plane (ξ, p_ξ), the motion occurs inside the two lines $\xi = \xi_1$ and ξ_2 (see Fig. 4). In the half-space $p_\xi > 0$, the particle moves toward the outer boundary, whereas for negative p_ξ, it travels in the direction of the inner boundary. The reflections of the momentum $p_\xi \to -p_\xi$ and $-p_\xi \to p_\xi$ at both boundaries correspond to vertical "jumps" along the dashed lines $\xi = \xi_1$ and ξ_2 connecting the upper and the lower level curves.

The values η_C and ξ_C of the caustics for L and R motions can be determined from Eq. (15) by setting $p_\eta = 0$ and $p_\xi = 0$, respectively. Thus

$$\eta_C = \arcsin(\mu_C) = \arccos\left(\frac{1}{\epsilon_C}\right), \tag{16a}$$

$$\xi_C = \operatorname{arcsinh}(\mu_C) = \operatorname{arccosh}\left(\frac{1}{\epsilon_C}\right), \tag{16b}$$

where the eccentricity ϵ_C and the parameter μ_C of the caustics are

$$\epsilon_C = \frac{f}{a_C} = \frac{1}{\sqrt{1+\gamma}}, \tag{17a}$$

$$\mu_C = \frac{b_C}{f} = \sqrt{|\gamma|}. \tag{17b}$$

A trajectory is in general open, that is, the particle never returns to the same point, and forms a dense subset of the region bounded by the caustic and the boundaries. For particular values of the constant γ, the trajectory closes and forms a polygon circumscribed about the caustic and inscribed in the elliptic boundaries. We study these periodic orbits in the next section.

III. THE PERIODIC ORBITS

The periodic orbits of the confocal elliptic billiard can be determined by introducing the action-angle variables[20,21] of the Hamilton–Jacobi theory given by

$$J_\xi(\gamma) = \frac{1}{2\pi} \oint p_\xi \, d\xi = 2\frac{Pf}{2\pi} \int_{\xi_{\min}}^{\xi_2} d\xi \sqrt{\sinh^2 \xi - \gamma}, \tag{18a}$$

$$J_\eta(\gamma) = \frac{1}{2\pi} \oint p_\eta \, d\eta = 4\frac{Pf}{2\pi} \int_{\eta_{\min}}^{\pi/2} d\eta \sqrt{\sin^2 \eta + \gamma}, \tag{18b}$$

where the integrals are over a complete period of the coordinates ξ and η. Given a value of γ, the actions J_ξ and J_η are proportional to the geometrical area enclosed by the corresponding orbits of the Poincaré maps depicted in Figs. 3 and 4. The corresponding lower limits of the integrals in Eq. (18) are given by

$$\begin{aligned} &\text{L-type,} \quad \xi_{\min} = \xi_1, \quad \eta_{\min} = \eta_C; \\ &\text{R1-type,} \quad \xi_{\min} = \xi_1, \quad \eta_{\min} = 0; \\ &\text{R2-type,} \quad \xi_{\min} = \xi_C, \quad \eta_{\min} = 0. \end{aligned} \tag{19}$$

The actions J_ξ and J_η in Eq. (18) are expressed explicitly in terms of elliptic integrals as follows. For librational orbits $(-1 \leqslant \gamma < 0)$ we have

$$J_\xi = \frac{P}{\pi} \sum_{j=1,2} (-1)^j \left[a_j \sin\theta_j - f\gamma F\left(\theta_j, \frac{1}{\epsilon_C}\right) - fE\left(\theta_j, \frac{1}{\epsilon_C}\right)\right], \tag{20a}$$

$$J_\eta = \frac{2Pf}{\pi}[\gamma K(1/\epsilon_C) + E(1/\epsilon_C)]. \tag{20b}$$

For R1 orbits $(0 < \gamma \leqslant \mu_1^2)$,

$$J_\xi = \frac{P}{\pi} \sum_{j=1,2} (-1)^j [a_j \sin\phi_j - a_C E(\phi_j, \epsilon_C)], \tag{21a}$$

$$J_\eta = \frac{2P}{\pi} a_C E(\epsilon_C). \tag{21b}$$

And for R2 orbits $(\mu_1^2 \leqslant \gamma \leqslant \mu_2^2)$,

$$J_\xi = \frac{P}{\pi}[a_2 \sin\phi_2 - a_C E(\phi_2, \epsilon_C], \tag{22a}$$

$$J_\eta = \frac{2P}{\pi} a_C E(\epsilon_C), \tag{22b}$$

where

$$\sin\phi_j = \frac{1}{\sin\theta_j} = \frac{1}{b_j}\sqrt{b_j^2 - f^2\gamma} = \sqrt{1 - \frac{\gamma}{\mu_j^2}}, \tag{23}$$

and,

$$F(\theta,m)=\int_0^{\theta}\frac{d\theta}{\sqrt{1-m^2\sin^2\theta}}, \tag{24a}$$

$$E(\theta,m)=\int_0^{\theta}d\theta\sqrt{1-m^2\sin^2\theta}, \tag{24b}$$

are the elliptic integrals of the first and second kind, respectively.[22] The corresponding complete integrals are denoted as $K(m)=F(\pi/2,m)$ and $E(m)=E(\pi/2,m)$.

As shown by Berry,[23] the periodic orbits of an integrable system can be found by the condition that the winding number $w=\omega_\eta/\omega_\xi$ be a rational number. Here ω_ξ and ω_η are the angular frequencies (angle variables conjugate to the actions) of the confocal elliptic billiard. In the present case we have

$$w=\frac{\omega_\eta}{\omega_\xi}=\frac{\dfrac{\partial H}{\partial J_\eta}}{\dfrac{\partial H}{\partial J_\xi}}=\frac{\partial J_\xi}{\partial J_\eta}=\frac{\left|\dfrac{\partial J_\xi}{\partial\gamma}\right|}{\left|\dfrac{\partial J_\eta}{\partial\gamma}\right|}=\frac{n}{r}, \tag{25}$$

where n and r are two integers. The periodic trajectory (n,r) closes after r periods of ξ and n periods of n. If the winding number is irrational, the orbit never goes back to the same point and forms a dense subset of the region between the caustics and the boundaries.

By differentiating J_ξ and J_η with respect to γ, we obtain for L motion

$$\frac{\partial J_\xi}{\partial\gamma}=-\frac{P}{2\pi f}[F(\theta_2,1/\epsilon_C)-\mathrm{F}(\theta_1,1/\epsilon_C)], \tag{26a}$$

$$\frac{\partial J_\eta}{\partial\gamma}=\frac{P}{\pi f}K(1/\epsilon_C), \tag{26b}$$

while for R1 motion,

$$\frac{\partial J_\xi}{\partial\gamma}=-\frac{P}{2\pi a_C}[F(\phi_2,\epsilon_C)-F(\phi_1,\epsilon_C)], \tag{27a}$$

$$\frac{\partial J_\eta}{\partial\gamma}=\frac{P}{\pi a_C}K(\epsilon_C), \tag{27b}$$

and for R2 motion,

$$\frac{\partial J_\xi}{\partial\gamma}=-\frac{P}{2\pi a_C}F(\phi_2,\epsilon_C), \tag{28a}$$

$$\frac{\partial J_\eta}{\partial\gamma}=\frac{P}{\pi a_C}K(\epsilon_C). \tag{28b}$$

We substitute the derivatives of the actions in Eq. (25) and obtain the characteristic equations for periodic orbits in the confocal elliptic billiard, namely

$$\text{L-type,}\quad w_{n,r}=\frac{n}{r}=\frac{F(\theta_2,1/\epsilon_C)-F(\theta_1,1/\epsilon_C)}{2\mathrm{K}(1/\epsilon_C)}, \tag{29a}$$

$$\text{R1-type,}\quad w_{n,r}=\frac{n}{r}=\frac{F(\phi_2,\epsilon_C)-F(\phi_1,\epsilon_C)}{2K(\epsilon_C)}, \tag{29b}$$

$$\text{R2-type,}\quad w_{n,r}=\frac{n}{r}=\frac{F(\phi_2,\epsilon_C)}{2K(\epsilon_C)}, \tag{29c}$$

where ϵ_C, θ_j, and ϕ_j depend on γ and the geometrical parameters of the billiard given by Eqs. (17) and (23).

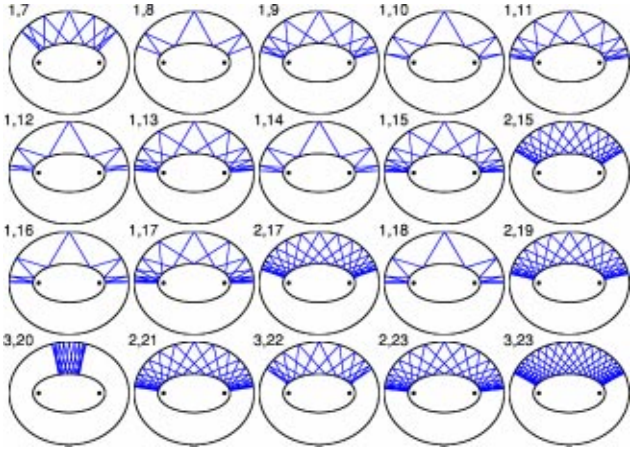

Fig. 5. Librational (L) orbits for a confocal elliptic billiard with $f=1$, $\xi_1=0.6$, and $\xi_2=1.3$. For these values $w_L=0.1502$.

Figures 5 and 6 show the first periodic tori for L and R1 motions in the confocal elliptic billiard. For a given winding number $w_{n,r}$, Eq. (29) uniquely determines the eigenvalue $\gamma_{n,r}$ for each kind of motion. The constant $\gamma_{n,r}$ is independent of the starting point of the orbit. Thus we can rotate the trajectory around the caustic by moving the initial point on the boundary, without changing its winding number. The orbits are chosen so that they are always symmetric to the y axis and, if possible, also to the x axis. For L motion the integer r counts the number of reflections at the outer boundary and n is the number of times that the orbit touches one of the caustics. For rotational motion r gives the number of reflections at the outer boundary, and n is the number of rotations about the origin. We have not shown periodic orbits for R2 motion because they are the same as the elliptic billiard and typical plots can be found elsewhere.[24]

In Fig. 7 we show the winding number in Eq. (29) as a function of γ for the three kinds of motion. Once $\gamma_{n,r}$ is calculated, the geometrical parameters of the caustic can be determined by using Eq. (17).

The isolated orbit (1,1) along the y axis and its repetitions $r(1,1)=(r,r)$ correspond to the end point of the librational region at $\gamma=-1$. Equation (29a) for the periodic orbits can be solved analytically for this value of γ. While so doing, we

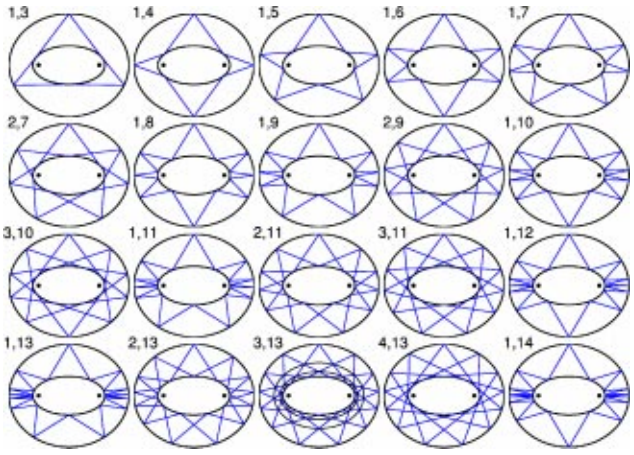

Fig. 6. Rotational (R1) orbits for a confocal elliptic billiard with $f=1$, $\xi_1=0.6$, and $\xi_2=1.3$. For these values $w_R=0.3594$.

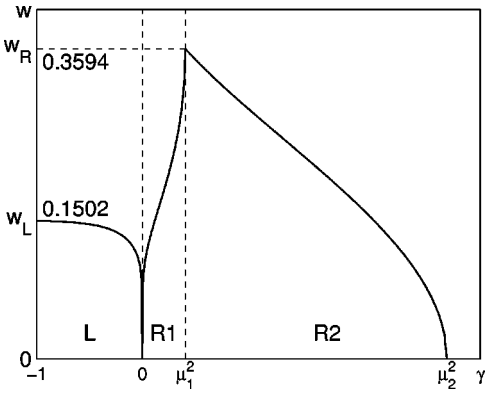

Fig. 7. Plot of the winding number $w(\gamma)$ for the three kinds of motion.

would notice that a librational torus (n,r) can occur in the billiard only if its $w_{n,r}$ satisfies the cutoff condition

$$w_{n,r} \leqslant w_L = \frac{\theta_2 - \theta_1}{\pi} = \frac{1}{\pi} \arcsin\left[\frac{f(b_2 - b_1)}{a_1 a_2}\right]. \tag{30}$$

Consider a librational orbit (n,r) in the confocal elliptic billiard. If we decrease w_L by changing the geometrical parameters of the billiard, the hyperbolic caustics become closer to each other, and the trajectory tightens about the y axis. The limit $w_L = w_{n,r}$ corresponds to the bifurcation points where the caustics coincide exactly with the y axis, and the torus (n,r) collapses to the isolated orbit $r(1,1)$. At each bifurcation point $w_L = w_{n,r}$, a new family of librational orbits $K(n,r) = (Kr,Kn)$ with Kr bounces is born.

The quantity $f(b_2 - b_1)/a_1 a_2$ in Eq. (30) ranges in the interval $[0,1)$, where the upper limit corresponds to the limiting case for which the inner boundary reduces to a point at the origin and the outer boundary becomes a circle. Now it is evident that w_L has the upper bound $w_{L,\max} = 1/2$, and consequently Eq. (29a) has periodic solutions for $r \geqslant 3$ and $n < r/2$. This fact leads us to conclude that the librational periodic orbit (1,2), for example, the bowtie orbit $\bowtie$) and its repetitions, cannot exist in the confocal elliptic billiard. We emphasize that the isolated orbit (1,1) is the only stable periodic orbit with $r < 3$.

On the other hand, a rotational torus (n,r) can occur in the billiard only if its winding number $w_{n,r}$ fulfills the condition

$$w_{n,r} \leqslant w_R = \frac{F(\arcsin\sqrt{1 - (b_1/b_2)^2}, \epsilon_1)}{2K(\epsilon_1)}. \tag{31}$$

Similar to w_L, the cusp w_R has the upper limit $w_{L,\max} = 1/2$. Thus the characteristic equations (29b) and (29c) have real solutions for integers (n,r) such that $r \geqslant 3$ and $n < r/2$. Physically, at least three outer reflections are required to complete a revolution in the confocal elliptic billiard. Only in the limit $r \to \infty$ can the winding number be zero. Because $w_R > w_L$ (see Fig. 7), not all rotational winding numbers exist for the librational case [for example, orbit (1,3) in Figs. 5 and 6].

Because the caustic is determined uniquely for a given winding number, we can choose any point on the outer boundary (evidently between caustics for L motion) as the initial vertex for the construction of the trajectory (see Fig. 8). Thus every point of the ellipse determines an orbit with the same number of sides and, as we will see, the same

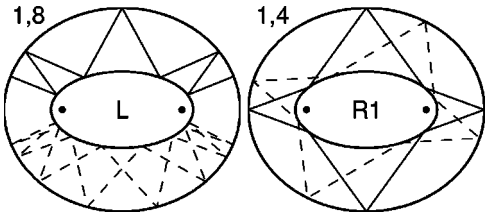

Fig. 8. Two examples of periodic tori in the confocal elliptic billiard. For each torus two periodic orbits are plotted (full and dashed lines). The length of the orbits remains constant independently of the starting point of the polygon.

length. This situation is typical of integrable systems: periodic tori are not isolated, but form a continuous family that fills configuration space. The length of the torus (n,r) is

$$L_{n,r} = \frac{2\pi}{P}(rJ_\xi + nJ_\eta), \tag{32}$$

where the actions are evaluated at $\gamma = \gamma_{n,r}$. If we substitute Eqs. (20)–(22) into Eq. (32), we obtain the following explicit expressions.

L motion:

$$L_{n,r} = 2r\left\{a_2 \sin\theta_2 - a_1 \sin\theta_1 - f\left[E\left(\theta_2, \frac{1}{\epsilon_C}\right) - E\left(\theta_1, \frac{1}{\epsilon_C}\right) - \frac{2n}{r}E\left(\frac{1}{\epsilon_C}\right)\right]\right\}. \tag{33a}$$

R1 motion:

$$L_{n,r} = 2r\left\{a_2 \sin\phi_2 - a_1 \sin\phi_1 - a_C\left[E(\phi_2, \epsilon_C) - E(\phi_1, \epsilon_C) - \frac{2n}{r}E(\epsilon_C)\right]\right\}. \tag{33b}$$

R2 motion:

$$L_{n,r} = 2r\left[a_2 \sin\phi_2 - \frac{f}{\epsilon_C}Z(\phi_2, \epsilon_C)\right], \tag{33c}$$

where $Z(\alpha,m) = E(\alpha,m) - F(\alpha,m)E(m)/K(m)$ is the Jacobi zeta function.[22]

From Eq. (33) we see that the lengths depend exclusively on $\gamma_{n,r}$. Therefore for a given torus (n,r), the length of the closed trajectories remain constant, independent of the starting point as shown in Fig. 8. This independence means that if a given orbit is periodic, all the other orbits on the same iso-γ curve also are periodic with the same period. If it is not periodic, the same will be true for all the orbits on the same iso-γ curve. Also, on each integral curve, the points of the orbits are ordered in the same way. All of these results are a consequence of Poncelet's theorem.[14] This theorem states that if, given two conics, there is a polygon having its vertices on one conic and sides tangent to the other, then there are an infinite number of polygons with the same property.[14] They all have the same number of sides and their vertices are ordered in the same way.

Now let us consider in more detail the stability of the isolated vertical and horizontal orbits (1,1) corresponding to $\gamma = -1$ and $\gamma = 0$, respectively. For both orbits the particle bounces alternately off both ellipses resembling the repeated reflections of a ray between the spherical mirrors of a laser

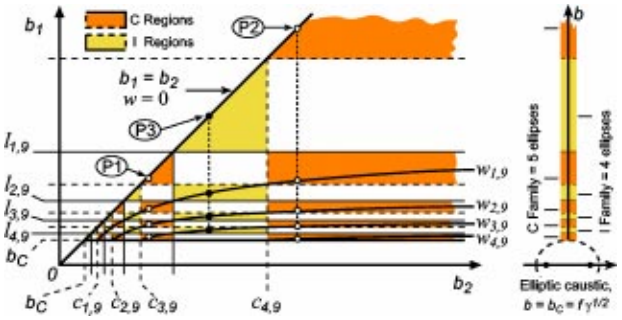

Fig. 9. Contour plot of the winding number w in the (b_1,b_2) plane for $\gamma=0.5$. The family of iso-w curves corresponds to constant values of $w_{n,r}$ for $n=\{1,2,3,4\}$, and $r=9$.

resonator. The stability condition is given by $0\leqslant g\leqslant 1$, where $g=(1-d/R_1)(1-d/R_2)$, with d the separation between impact points and R_1 and R_2 the radii of curvature at impact. The parameter g can be expressed explicitly in terms of the geometrical parameters of the billiard. For the vertical and horizontal orbits we obtain

$$g_v=\left(\frac{f^2+b_1b_2}{a_1a_2}\right)^2<1, \tag{34a}$$

$$g_h=\left(\frac{f^2+a_1a_2}{b_1b_2}\right)^2>1. \tag{34b}$$

We can then confirm that the vertical orbit is stable, whereas the horizontal orbit is unstable. Similar results were obtained by Berry[8] for the simple elliptic billiard.

IV. GEOMETRICAL CONSTRUCTIONS FOR PERIODIC ORBITS

So far we have found the motion of a particle for a given billiard geometry. Our task has consisted of finding the eigenvalue of the constant of motion $\gamma_{n,r}$ for a particular orbit (n,r), that is, winding number $w_{n,r}=n/r$. However, we notice in the characteristic equation (29) that the winding number actually depends on four parameters, namely $w=w(b_1,b_2,\gamma,f)$. With this in mind, the original billiard problem may be inverted and restated as follows: Given γ and f, find one or more pairs of semiaxes (b_1,b_2) that satisfy Eq. (29) for an orbit (n,r). This new approach allows us to translate simple analytical properties of Eq. (29) into interesting geometrical constructions for the confocal elliptic billiard. For example, for the orbit (3,13) in Fig. 6, we note that the trajectory self-intersects in a number of cross-points that lie on two internal ellipses. We then identify four confocal ellipses that may be combined in pairs to construct six different confocal elliptic billiards. It is easy to recognize in this set of confocal elliptic billiards three orbits (1,13), two orbits (2,13), and the original orbit (3,13). Of course, all of these orbits share the same γ. Some relevant questions include what is the eccentricity of these internal ellipses? If we extend the line segments of the original trajectory (3,13), is it possible to find more external ellipses beyond the outer boundary or internal ellipses inside the inner boundary?

To treat these questions we need to deal with the characteristic equation (29b) for R1 motion. Deeper dynamical insight is gained by plotting the winding number w in the (b_1,b_2) plane for fixed γ (see Fig. 9). The family of iso-w curves corresponds to constant values of $w_{n,r}$ in Eq. (29b) for $n=\{1,2,3,4\}$, and $r=9$. Evidently, the region of interest is delimited by the conditions $b_1\geqslant b_C=f\gamma^{1/2}$ and $b_2\geqslant b_1$. Each point on the curve $w_{n,r}$ represents a distinct combination of semiaxes b_1 and b_2 of the confocal elliptic billiard such that the periodic orbit (n,r) exists for the given γ. The winding number w is the interval $0\leqslant w<1/2$, where the level curve $w=0$ corresponds to the straight line $b_2=b_1$, and the limit $w\to 1/2$ is reached when $b_1=b_C$ and b_2 go to infinity. Because $w(b_1,b_2)$ is a monotonically varying surface, two iso-w curves cannot intersect.

We discuss some of the geometrical properties of the iso-w curves. Level curves $w_{n,r}$ are "born" at the cutoff points $b_2=c_{n,r}$ on the horizontal line $b_1=b_C$ and increase asymptotically to the limits $b_1=l_{n,r}$ as b_2 goes to infinity. The values of the cutoffs $c_{n,r}$ and limits $l_{n,r}$ can be readily obtained from Eq. (29b), namely

$$c_{n,r}=\frac{b_C}{\mathrm{cn}(2w_{n,r}K(\epsilon_C))}, \tag{35a}$$

$$l_{n,r}=\frac{b_C}{\mathrm{cn}((1-2w_{n,r})K(\epsilon_C))}, \tag{35b}$$

where cn is the cosine-like Jacobian elliptic function, and b_C and ϵ_C are given in terms of γ and f by Eq. (17).

Let us first assume that the number of reflections r is odd. In this case, the cutoffs and limits can be sorted as follows:

$$b_C<l_{n_{\max},r}<c_{1,r}<l_{n_{\max-1},r}<c_{2,r}<\cdots<l_{1,r}<c_{n_{\max},r}<\infty, \tag{36}$$

where $n_{\max}=(r-1)/2$. If we arrange these values along both axes and trace solid lines for the limits and dashed lines for the cutoffs, the (b_2,b_1) plane may be divided into regions, denoted as C and I in Fig. 9. The $C(I)$ regions are delimited at the top and right sides by limits (cutoffs) and at the bottom and left sides by cutoffs (limits). Note that the C regions for $b>c_{n_{\max},r}$ extend indefinitely.

Given an initial elliptic boundary with semiminor axis b_0, Fig. 9 can be used to find the entire family of confocal ellipses for which orbits (1,9),...,(4,9) exist. To do this, we first locate the value b_0 on the $b_1=b_2$ line (for example, point P1 in Fig. 9), and then draw a horizontal and a vertical line starting from this point. The intersections of these lines with the iso-w curves define the semiaxes b of the desired ellipses. We identify two cases.

(1) C family: When b_0 lies in a C region (for example, points P1 or P2), there are $n_{\max}+1$ intersections (white circles), including the curve $w=0$. Consequently a C family is composed by $n_{\max}+1$ confocal ellipses, as shown in Fig. 10(a) for $r=9$ and $n_{\max}=4$.
(2) I family: When b_0 lies in a I region (for example, point P3), there are only $n_{\max}$ intersections (black circles), and consequently, $n_{\max}$ confocal ellipses [see Fig. 10(b)].

On the right-hand side of Fig. 9, we notice that by putting in ascending order the values $c_{n,r}$ and $l_{n,r}$ along a single b-axis, this axis is divided into a set of $(n_{\max}+1)$ C-bands and a set of $n_{\max}$ I-bands.

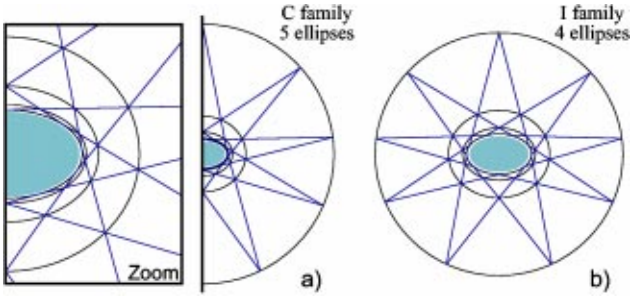

Fig. 10. Construction of C and I families of confocal elliptic billiards for $r=9$. The zoom shows the C trajectories in greater detail.

The above results are valid when the number of reflections r is odd. If r is even, the cutoffs and limits Eq. (35) satisfy the sequence

$$b_C<l_{n_{\max},r}=c_{1,r}<l_{n_{\max-1},r}=c_{2,r}<\cdots<l_{1,r}=c_{n_{\max},r}, \tag{37}$$

where now $n_{\max}=(r-2)/2$. The iso-w curves in Fig. 9 have the same behavior, except for the fact that two consecutive solid and dashed lines coincide, such that the I regions vanish. As a result, for even values of r, it is always possible to find $n_{\max}+1=r/2$ confocal ellipses.

The geometrical constructions discussed in this section for rotational motion can be extended without any difficulty to orbits exhibiting librational motion. In this case we need to deal with Eq. (29a). Now the corresponding cutoffs $c_{n,r}$ and limits $l_{n,r}$ are given by

$$c_{n,r}=b_C\mathrm{sc}(2w_{n,r}K(1/\epsilon_C)), \tag{38}$$

$$l_{n,r}=b_C\mathrm{sc}((1-2w_{n,r})K(1/\epsilon_C)), \tag{39}$$

where sc=sn/cn is a Jacobian elliptic function. The iso-w curves in the (b_1,b_2) plane for fixed γ behave very similarly to the iso-w curves depicted in Fig. 9 for the rotational case. For L motion we also can construct C families composed of $n_{\max}+1$ of confocal ellipses and I families composed of $n_{\max}$ ellipses if r is odd. For even values of r only C families can be found.

V. CONCLUSIONS

We have derived the conditions for stable periodic trajectories within a confocal elliptic billiard. This analysis revealed the existence of three kinds of motion: one librational and two rotational. Because the system is simple, it has been possible to find explicit characteristic equations for the periodic orbits in terms of the geometrical parameters and the constants of motion. Plots of the winding number on the (b_1,b_2) plane lets us gain a deeper insight into the dynamics of the billiard. Because this paper is relatively self-contained, we believe that students can take our results as a starting point to explore numerically the properties of elliptic integrals and how they predict interesting geometrical properties of the orbits inside the billiard.

ACKNOWLEDGMENTS

The authors wish to acknowledge financial support from Consejo Nacional de Ciencia y Tecnología, México under Grant No. I-36456, and from Tecnológico de Monterrey (Research Chair in Optics) under Grant No. CAT-007.

[a]Electronic mail: juliocesar@itesm.mx

[1]M. C. Gutzwiller, *Chaos in Classical and Quantum Mechanics* (Springer, New York, 1990).
[2]M. F. Crommie, C. P. Lutz, and D. M. Eigler, "Confinement of electrons to quantum corrals on a metal surface," Science **262**, 218–223 (1993).
[3]R. W. Robinett, "Visualizing the solutions for the circular infinite well in quantum and classical mechanics," Am. J. Phys. **64**, 440–446 (1996).
[4]R. W. Robinett, "Visualizing classical periodic orbits from the quantum energy spectrum via the Fourier transform: Simple infinite well examples," Am. J. Phys. **65**, 1167–1175 (1997).
[5]R. W. Robinett, "Periodic orbit theory analysis of the circular disk or annular billiard: Nonclassical effects and the distribution of energy eigenvalues," Am. J. Phys. **67**, 67–77 (1999).
[6]E. Arcos, G. Báez, P. A. Cuatláyol, M. L. H. Prian, R. A. Méndez-Sánchez, and H. Hernández-Saldaña, "Vibrating soap films: An analog for quantum chaos on billiards," Am. J. Phys. **66**, 601–607 (1998).
[7]D. L. Kaufman, I. Kosztin, and K. Schulten, "Expansion method for stationary states of quantum billiards," Am. J. Phys. **67**, 133–141 (1999).
[8]M. V. Berry, "Regularity and chaos in classical mechanics, illustrated by three deformations of a circular billiard," Eur. J. Phys. **2**, 91–102 (1981).
[9]R. L. Liboff, *Introductory Quantum Mechanics*, 2nd ed. (Addison-Wesley, Reading, MA, 1991).
[10]C. Cohen-Tannoudji, B. Diu, and F. Laloë, *Quantum Mechanics* (Wiley, New York, 1977).
[11]J. Zhang, A. C. Merchant, and W. D. M. Rae, "Geometric derivations of the second constant of motion for an elliptic billiard and other results," Eur. J. Phys. **15**, 133–138 (1994).
[12]B. Crespi, S. J. Chang, and K. Shi, "Elliptical billiards and hyperelliptic functions," J. Math. Phys. **34**, 2257–2289 (1993).
[13]J. C. Gutiérrez-Vega, S. Chávez-Cerda, and R. M. Rodríguez-Dagnino, "Probability distributions in quantum and classical elliptic billiards," Rev. Mex. Fis. **47**, 480–488 (2001).
[14]S. J. Chang and R. Friedberg, "Elliptical billiards and Poncelet's theorem," J. Math. Phys. **29**, 1537–1550 (1988).
[15]M. Sieber, "Semiclassical transition from an elliptical to an oval billiard," J. Phys. A **30**, 4563–4596 (1997).
[16]J. Koiller, R. Markarian, S. O. Kamphorst, and S. Pinto de Carvalho, "Static and time-dependent perturbations of the classical elliptical billiard," J. Stat. Phys. **83**, 127–142 (1996).
[17]E. Y. Amiran, "Integrable smooth planar billiards and evolutes," New York J. Math. **3**, 32–47 (1997).
[18]D. A. Poet and R. R. W. Poet, "Confocal conic billiards," Phys. Lett. A **271**, 277–284 (2000).
[19]C. Foltin, "Billiards with positive topological entropy," Nonlinearity **15**, 2053–2076 (2002).
[20]H. Goldstein, *Classical Mechanics*, 2nd ed. (Addison-Wesley, Boston, 1980).
[21]A. L. Fetter and J. D. Walecka, *Theoretical Mechanics of Particles and Continua* (McGraw-Hill, New York, 1980).
[22]M. Abramowitz and I. Stegun, *Handbook of Mathematical Functions* (Dover, New York, 1964).
[23]M. V. Berry and M. Tabor, "Closed orbits and the regular bound spectrum," Proc. R. Soc. London, Ser. A **349**, 101–123 (1976).
[24]H. Waalkens, J. Wiersig, and H. R. Dullin, "Elliptic quantum billiard," Ann. Phys. (N.Y.) **260**, 50–90 (1997).